[Note: this is a preprint and there may be minor differences with the journal version].

Interfacial and bulk polaron masses in Zn$_{1-x}$Mg$_x$O/ZnO heterostructures examined by terahertz time-domain cyclotron spectroscopy

J. Lloyd-Hughes,[1, a)] M. Failla,[1] J. Ye,[2, 3, b)] S. P. P. Jones,[4] K. L. Teo,[5] and C. Jagadish[3]

[1)] *University of Warwick, Department of Physics, Gibbet Hill Road, Coventry, CV4 7AL, United Kingdom.*

[2)] *School of Electronics, Science and Engineering, Nanjing University, Nanjing 210093, China*

[3)] *Department of Electronic Materials Engineering, Research School of Physical Sciences and Engineering, The Australian National University, Canberra ACT 0200, Australia*

[4)] *University of Oxford, Department of Physics, Clarendon Laboratory, Parks Road, Oxford, OX1 3PU, United Kingdom.*

[5)] *Department of Electrical and Computer Engineering, National University of Singapore, 117576, Singapore*

(Dated: 11 August 2015)

The cyclotron resonance of polarons in Zn$_{1-x}$Mg$_x$O/ZnO heterostructures (with $0.15 < x < 0.22$) was studied by terahertz time-domain spectroscopy. Low-temperature magnetoconductivity spectra of the 2D electron gas at the Zn$_{1-x}$Mg$_x$O/ZnO interface determined the polaron density, mass and scattering rate. The cyclotron mass of 2D polarons was found to increase significantly with magnetic field B from $0.24\,m_e$ at $B = 2\,\text{T}$ to $0.37\,m_e$ at $B = 7.5\,\text{T}$. A nonlinear cyclotron frequency with B was also observed for 3D polarons in ZnO. The findings are discussed in the context of polaron mass renormalization driven by the electron-LO-phonon and electron-acoustic phonon interactions.

a)Electronic mail: j.lloyd-hughes@warwick.ac.uk

b)Electronic mail: yejd@nju.edu.cn

Substantial interest in 2D electron gases and liquids in oxide heterostructures is motivated by reports of the quantum and fractional quantum Hall effect in $Zn_{1-x}Mg_xO/ZnO$ heterostructures,[1,2] and by novel phenomena at the $LaAlO_3/SrTiO_3$ interface.[3,4] In polar materials with significant electron-phonon coupling, such as ZnO, charges distort the lattice, forming *polarons*. The bare effective mass m_b^* is therefore altered to m^*.

For 3D polarons the mass enhancement factor is given by $m^*/m_b^* \simeq 1 + \alpha/6$, for small values of the electron-LO phonon coupling constant α. A comparison of the polaron mass from cyclotron resonance (CR)[5] ($m^* = 0.29\,m_e$) and the bare electron mass from Faraday rotation[6] at optical wavelengths ($m_b^* \simeq 0.24\,m_e$) yields $\alpha \simeq 1.2$ for bulk ZnO. The polaron mass has been found to be enhanced for 2D polarons in ZnO: for instance, CR experiments below $400\,\text{GHz}$ and for $B < 4\,\text{T}$ found $m^* = 0.30\,m_e$ for $Zn_{1-x}Mg_xO/ZnO$ 2DEGs with $n < 1.2 \times 10^{12}\,\text{cm}^{-2}$,[7] while $m^* = 0.32\,m_e$ was reported for $n \simeq 6 \times 10^{12}\,\text{cm}^{-2}$.[8,9]

In this Article we report a study of the mass of interfacial polarons in $Zn_{1-x}Mg_xO/ZnO$ heterostructures, and of bulk-like polarons in a ZnO thin film. Terahertz time-domain cyclotron spectroscopy revealed a nonlinear dependence of the cyclotron frequency upon magnetic field that indicates strong changes in the polaronic mass. Resonant Raman and photoluminescence spectroscopies were used to assess phonon frequencies, the Mg content, and its compositional variation.

$Zn_{1-x}Mg_xO/ZnO$ heterostructures were grown on $c-$plane sapphire by metal-organic vapor phase epitaxy.[10,11] A thin ($0.48\,\mu\text{m}$) ZnO layer grown at low temperature was deposited first on the sapphire substrates, before a $3.34\,\mu\text{m}$-thick nominally-undoped ZnO template with Zn-termination.[10,11] A series of samples with $Zn_{1-x}Mg_xO$ top layers of different thicknesses from $25\,\text{nm}$ to $126\,\text{nm}$ were then grown on top of the ZnO. Due to the compositional pulling effect, a compositionally graded $Zn_{1-x}Mg_xO$ layer was formed at the interface, with a thickness of about $10\,\text{nm}$.[11] A piece of the ZnO/LT-ZnO/sapphire wafer without a $Zn_{1-x}Mg_xO$ layer acted as a reference. A UV He-Cd laser ($325\,\text{nm}$; $3.82\,\text{eV}$) was used to perform resonant Raman spectroscopy and photoluminescence (PL) at sample temperatures of $77\,\text{K}$, to estimate x.

The PL spectra reported in Fig. 1(a) show strong excitonic emission from the ZnO layer, peaking at the donor-bound exciton energy $E_{\text{DX}} = 3.37\,\text{eV}$, and LO-phonon replica at energies $E_{\text{DX}} - n\hbar\omega_{\text{LO}}$ (for $n \leq 4$, $\hbar\omega = 71\,\text{meV}$). The $Zn_{1-x}Mg_xO$ layers emit at higher energies, with a bandgap that increases with x.[12] The bandgap energy for $x \sim 0.21$ ($126\,\text{nm}$

sample) is $\sim 3.7\,\text{eV}$. The PL spectra of the $\text{Zn}_{1-x}\text{Mg}_x\text{O}$ layers are broad as a result of compositional grading.[11] No excitonic PL emission was witnessed from the $\text{Zn}_{1-x}\text{Mg}_x\text{O}$ layers, which may be a result of electric-field-induced exciton dissociation[13] in the surface electric field of $\text{Zn}_{1-x}\text{Mg}_x\text{O}$.

The $A_1(\text{LO})$ phonon was observed using resonant Raman scattering, and is labelled "1LO" in Fig. 1(b). This phonon blueshifts with increasing x, in agreement with previous studies,[14,15] and as a consequence of the compressive strain of Zn-O bonds in $\text{Zn}_{1-x}\text{Mg}_x\text{O}$.[15] A $26\,\text{cm}^{-1}$ increase in $A_1(\text{LO})$ frequency observed for the $25\,\text{nm}$ $\text{Zn}_{1-x}\text{Mg}_x\text{O}$ layer permits an estimate of $x \lesssim 0.18 \pm 0.02$ based on Ref. 14. The second-order "2LO" Raman peak at the second harmonic of the $A_1(\text{LO})$ and $E_1(\text{LO})$ frequencies[16] is likewise blueshifted.

The bandstructure of the $25\,\text{nm}$ $\text{Zn}_{0.84}\text{Mg}_{0.16}\text{O}$ layer was calculated using a self-consistent solution to the Schrödinger-Poisson equation, and is reported in Fig. 2. Here, a linear gradation of the $\text{Zn}_{1-x}\text{Mg}_x\text{O}$ from $x = 0.16$ to $x = 0.0$ over the last $10\,\text{nm}$ of the $\text{Zn}_{1-x}\text{Mg}_x\text{O}$ film was assumed. The electronic wavefunction (solid blue line) straddles both the $\text{Zn}_{1-x}\text{Mg}_x\text{O}$ and ZnO. The calculated carrier density (shaded area) is consistent with the experimental result (points) derived from a capacitance-voltage measurement.

Terahertz time-domain spectroscopy[17,18] was utilized to determine the complex magneto-conductivity in the frequency range $100\,\text{GHz} < \omega/2\pi < 2\,\text{THz}$. Samples were placed in the variable-temperature insert of a split-coil superconducting magnet, which applied a magnetic field B along the c-axis. The diagonal components $\sigma_{xx}(\omega)$ of the complex magnetoconductivity tensor were determined. In Fig. 3(a) the amplitude of the complex THz transmission $|T(\omega)| = |E_s(\omega, B)/E_r(\omega, B)|$ is reported for a $126\,\text{nm}$-thick $\text{Zn}_{1-x}\text{Mg}_x\text{O}/\text{ZnO}$ heterostructure at $2\,\text{K}$. Here, E_s is the amplitude spectrum of the THz pulse transmitted through the heterostructure sample, while E_r is the spectral amplitude transmitted through the ZnO reference. Thus, only carriers in the 2DEG influence the transmission.

Without a magnetic field the minimum in the transmission is at zero frequency, while at $B = 5\,\text{T}$ the resonance shifts to $1.8\,\text{meV}$ ($0.43\,\text{THz}$). The magnetoconductivity $\sigma_{xx}(\omega, B)$ was calculated directly from the complex transmission $T(\omega)$ using the thin-film limit,[18] and assuming a THz dielectric constant $\epsilon_s = 10.8$ for the $\text{Zn}_{1-x}\text{Mg}_x\text{O}$ and ZnO layers. In Fig. 3(b) the real part of the magnetoconductivity σ_1 is reported. The spectral weight $S = \int_0^\infty \sigma_1 d\omega$ at $B = 5\,\text{T}$ is lower than that at zero magnetic field. The optical sum rule for the electron density, $N = 2m^*S/\pi e^2$, therefore indicates that the effective mass m^* at $B = 5\,\text{T}$ is higher

than at $B = 0\,\mathrm{T}$ (assuming constant density).

Transmission spectra were modelled using the transfer matrix method, assuming an interfacial 2DEG on the $\mathrm{Zn}_{1-x}\mathrm{Mg}_x\mathrm{O}/\mathrm{ZnO}$ boundary with a magnetoconductivity given by the Drude-Lorentz formalism,[18] and an electron sheet density $n = 2.2 \times 10^{12}\,\mathrm{cm}^{-2}$ ($126\,\mathrm{nm}$ $\mathrm{Zn}_{1-x}\mathrm{Mg}_x\mathrm{O}$) or $n \simeq 1 \times 10^{12}\,\mathrm{cm}^{-2}$ ($25\,\mathrm{nm}$ $\mathrm{Zn}_{1-x}\mathrm{Mg}_x\mathrm{O}$). This latter value is in accord with the calculated and experimental sheet density in Fig. 2. The solid lines in Fig. 3(a) indicate the fitted transmission with $m^* = 0.18 \pm 0.01 m_e$ (from the optical sum rule) and $\tau = 450 \pm 30\,\mathrm{fs}$ for $B = 0$, and $m^* = 0.31 \pm 0.01 m_e$ and $\tau = 700 \pm 30\,\mathrm{fs}$ for $B = 5\,\mathrm{T}$. In Fig. 3(b) these fitted values are used to plot σ_1 for the 2DEG layer (solid lines), which are in excellent agreement with σ_1 calculated directly from the transmission using the thin-film conductivity expression (points). The mobility calculated from the fit at $B = 0\,\mathrm{T}$ is $4400 \pm 400\,\mathrm{cm^2V^{-1}s^{-1}}$.

In order to examine the effective mass of bulk-like polarons the transmission of the ZnO reference sample was determined in relation to its value at zero magnetic field (i.e. $T' = E_r(B)/E_r(B = 0)$), as reported in Fig. 4. A temperature of $100\,\mathrm{K}$ was chosen to allow a sufficient population of extrinsic electrons in the n-type layer, at the maximum mobility of bulk ZnO.[19] Rather than minima that are symmetric about the CR frequency, as in Fig. 3(a), the spectra in Fig. 4 are asymmetric, with maxima towards zero frequency (as $|E_r(B = 0)|$ has a minimum at zero frequency, while at finite B the CR is at finite frequency). As the film's thickness ($3.82\,\mu\mathrm{m}$) is in the regime of intermediate optical thickness (between the thin and thick limits), the magnetoconductivity cannot be analytically calculated from the transmission. Therefore the transfer matrix method was again used to model T' assuming the Drude-Lorentz magnetoconductivity for the ZnO layer. The solid lines in Fig. 4 show fits to T' using $N = 1.6 \times 10^{17}\,\mathrm{cm}^{-3}$ for all data sets, and allowing m^* and τ to vary. Fits assuming constant $m^* = 0.29\,m_e$ but allowing N and τ to vary (e.g. dashed curve for $B = 3\,\mathrm{T}$) produced substantially poorer results. The scattering times obtained are $\tau \simeq 2\,\mathrm{ps}$.

The CR frequencies $\omega_c = eB/m^*$ and cyclotron masses $m^* = eB/\omega_c$ are reported in Figs. 5(a) and (b), respectively, for two $\mathrm{Zn}_{1-x}\mathrm{Mg}_x\mathrm{O}/\mathrm{ZnO}$ heterostructures and the bulk-like layer. The CR frequency for interfacial polarons in the $126\,\mathrm{nm}$ ZnMgO/ZnO sample (circles) increases nonlinearly with magnetic field, with masses increasing from $m^* = 0.25\,m_e$ at $B = 2\,\mathrm{T}$ to $m^* = 0.37\,m_e$ at $B = 7.5\,\mathrm{T}$. This is in line with the increase in m^* derived from the spectra as discussed above in reference to Fig. 3. The $25\,\mathrm{nm}$ ZnMgO/ZnO sample (triangles) also showed enhancements in m^* with B. The 3D polarons in the ZnO thin film

at 100 K showed substantially lower effective masses, and also exhibited an increase in m^* with B.

In the following we consider mechanisms that may account for the observed nonlinear $\omega_c(B)$. The electron mass can be altered by (i) the nonparabolicity of the conduction band, (ii) the electron-electron interaction (EEI), and (iii) the degree of spin-polarization. Further, ω_c is not proportional to B for (iv) defect-bound states. The polaron mass m^* depends on B in a way that differs for (v) the electron-LO phonon and (vi) the electron-longitudinal acoustic (LA) phonon interactions.

(i) At large electron energies the nonparabolicity of the conduction band alters m_b^* away from its Γ-point value. For 3D electrons, m_b^* increases from $m_b^* = 0.23\,m_e$ for $N = 6 \times 10^{17}\,\text{cm}^{-3}$ to $m_b^* = 0.35\,m_e$ at $N = 7 \times 10^{20}\,\text{cm}^{-3}$.[20,21] The enhancement in the band mass from nonparabolicity was estimated from a two-band Kane model.[22] Using the 2D Fermi energy of the 126 nm $\text{Zn}_{1-x}\text{Mg}_x\text{O}/\text{ZnO}$ 2DEG this yielded an increase of only 1 %. Similarly, no enhancement in m_b^* from nonparabolicity was found for the bulk-like electrons ($N = 1.8 \times 10^{17}\,\text{cm}^{-3}$). Nonparabolicity therefore cannot account for the enhancement in m^* with B.

(ii) The transport mass m_{tr}^* (from the temperature-dependent Shubnikov-de Haas amplitude) can be altered by the EEI, and is enhanced in ZnO 2DEGs at low densities.[7,23] Here, m_{tr}^* for the 25 nm $\text{Zn}_{1-x}\text{Mg}_x\text{O}/\text{ZnO}$ 2DEG was found to increase from $m_{\text{tr}}^* = 0.55 \pm 0.07\,m_e$ at $B = 5\,\text{T}$ to $m_{\text{tr}}^* = 0.65 \pm 0.07\,m_e$ at $B = 7.5\,\text{T}$. The electron-electron coupling constant was estimated as $\lambda_{e-e} = m_{\text{tr}}^*/m^* - 1 = 0.7, 0.9 \pm 0.1$ at $B = 5, 7.5\text{T}$, suggesting that electron correlations are strong in this system.[7] However, assuming the validity of Kohn's theorem[24,25] the EEI does not alter the CR frequency, and should not account for the change in the cyclotron mass m^* with field.

(iii) The renormalization of the effective mass in Fermi liquids can be influenced by the degree of spin-polarization via the exchange interaction.[26,27] The $\text{Zn}_{1-x}\text{Mg}_x\text{O}/\text{ZnO}$ heterostructures studied herein were found to be spin polarized and to exhibit weak ferromagnetism.[11,28] However, the magnetization saturated at $B = 0.4\,\text{T}$, and the degree of spin-polarization should therefore not alter at the magnetic field strengths $B > 1\,\text{T}$ used in the CR experiments.

(iv) CR studies on bulk ZnO at 4.2 K and 60 K reported transitions associated with electrons bound to shallow traps,[5] with zero-field cyclotron energies of 2.5 meV and 7.8 meV,

and also at 5.9 meV and 7.2 meV.[29] No such hydrogenic (1s-2p) transitions[30] were observed in the present study, as the $B = 0$ limit of the observed cyclotron energies was $\hbar\omega_c = 0$.

(v) Magnetopolarons produce nonlinear $\omega_c(B)$ relations, as reported in other wide bandgap polar materials.[31] The electron-LO phonon interaction in a magnetic field enhances the mass of 2D polarons.[32] In the weak coupling limit (small α) and at small B the renormalized mass is

$$m^* = m_b^*(1 + \frac{\pi\alpha}{8} + \frac{9\pi\alpha}{64}\frac{eB}{m_b^*\omega_{LO}}),\tag{1}$$

For larger α and B the function $\omega_c(B)$ maps out a typical anti-crossing dispersion,[33] with the lower magnetopolaron branch tending to ω_{LO} as $B \to \infty$. Since the lowest LO-phonon frequency (A_1, at $\omega_{LO} = 583\,\mathrm{cm}^{-1}$) is high the CR mass is not affected by the LO-phonon-CR anti-crossing at low magnetic fields.

(vi) In piezoelectric materials, the electron-LA phonon interaction alters the cyclotron frequency,[34,35] for instance as reported for bulk n-type CdS in the quantum limit ($\hbar\omega_c > k_B T$).[36] In contrast to the electron-LO phonon interaction, which lowers E_{CR} (increases m_{CR}^*), the electron-LA phonon interaction enhances E_{CR} (lowers m^*) at low magnetic fields[35] according to

$$\omega_c = \frac{eB}{m_p^*}(1 + X\alpha_{ac}Tm_p^*B^{-3/2}),\tag{2}$$

where m_p^* is the polaron mass (including the LO-phonon interaction), α_{ac} is the electron-acoustic phonon coupling constant, and $X = 0.665e^{-3/2}\hbar^{-1/2}k_B\epsilon^{-1}a_B^{-1}$ for Bohr radius $a_B = 52.9\,\mathrm{pm}$ and dielectric constant perpendicular to the c-axis $\epsilon = 7.4$. The solid blue, green and red lines for $\omega_c(B)$ and $m^*(B)$ reported in Fig. 5 were calculated with $T = 2, 2, 100\,\mathrm{K}$, $m_p^* = 0.38, 0.35, 0.29\,m_e$ and $\alpha_{ac} = 0.4, 0.4, 0.008$, respectively, to fit the 126 nm $Zn_{1-x}Mg_xO/ZnO$, 25 nm $Zn_{1-x}Mg_xO/ZnO$ and bulk-like ZnO data sets. The model shows reasonable agreement with experiment for realistic values of the polaron mass, particularly given the assumption in the model that only the lowest Landau level was occupied.[35] In contrast, for CdS with $m_p^* = 0.20\,m_e$, $\alpha_{ac} = 0.035$.[34,35]

In summary, the effective mass, density and scattering rate of bulk-like (3D) polarons and interfacial (2D) polarons in $Zn_{1-x}Mg_xO/ZnO$ thin film heterostructures was studied by THz time-domain spectroscopy. The effective mass was suppressed below the bulk value at low magnetic fields, and increased with applied field. Possible origins of the observed effect were discussed, and the electron-acoustic phonon interaction was identified as playing

a prominent role.

REFERENCES

[1] A. Tsukazaki, A. Ohtomo, T. Kita, and Y. Ohno, Science **315**, 1388 (2007).

[2] A. Tsukazaki, S. Akasaka, K. Nakahara, Y. Ohno, H. Ohno, D. Maryenko, A. Ohtomo, and M. Kawasaki, Nature Mater. **9**, 889 (2010).

[3] A. Ohtomo and H. Y. Hwang, Nature **427**, 423 (2004).

[4] N. Reyren, S. Thiel, A. D. Caviglia, L. F. Kourkoutis, G. Hammerl, C. Richter, C. W. Schneider, T. Kopp, A. S. Ruetschi, D. Jaccard, et al., Science **317**, 1196 (2007).

[5] Y. Imanaka, M. Oshikiri, K. Takehana, T. Takamasu, and G. Kido, Physica B: Cond. Mat. **298**, 211 (2001).

[6] W. Baer, Phys. Rev. **154**, 785 (1967).

[7] Y. Kasahara, Y. Oshima, J. Falson, Y. Kozuka, A. Tsukazaki, M. Kawasaki, and Y. Iwasa, Phys. Rev. Lett. **109**, 246401 (2012).

[8] Y. Imanaka, T. Takamasu, H. Tampo, H. Shibata, and S. Niki, Physica Stat. Sol. C **7**, 1599 (2010).

[9] Y. Imanaka, J. Low Temp. Phys. **170**, 389 (2012).

[10] J. D. Ye, S. Pannirselvam, S. T. Lim, J. F. Bi, X. W. Sun, G. Q. Lo, and K. L. Teo, Appl. Phys. Lett. **97**, 111908 (2010).

[11] J. Ye, S. Ter Lim, M. Bosman, S. Gu, Y. Zheng, H. H. Tan, C. Jagadish, X. Sun, and K. L. Teo, Sci. Rep. **2**, 533 (2012).

[12] J. Kang, Y. Park, and K. Kim, Sol. Stat. Comms. **115**, 127 (2000).

[13] J. Lloyd-Hughes, T. Richards, H. Sirringhaus, M. B. Johnston, and L. M. Herz, Phys. Rev. B **77**, 125203 (2008).

[14] J. D. Ye, K. W. Teoh, X. W. Sun, G. Q. Lo, D. L. Kwong, H. Zhao, S. L. Gu, R. Zhang, Y. D. Zheng, S. A. Oh, et al., Appl. Phys. Lett. **91**, 091901 (2007).

[15] J. F. Kong, W. Z. Shen, Y. W. Zhang, C. Yang, and X. M. Li, Appl. Phys. Lett. **92**, 191910 (2008).

[16] R. Cuscó, E. Alarcón-Lladó, J. Ibáñez, L. Artús, J. Jiménez, B. Wang, and M. Callahan, Phys. Rev. B **75**, 165202 (2007).

[17] J. Lloyd-Hughes and T.-I. Jeon, J Infrared Milli Terahz Waves **33**, 871 (2012).

[18] J. Lloyd-Hughes, J. Phys. D: Appl. Phys. **47**, 374006 (2014).

[19] J. B. Baxter and C. A. Schmuttenmaer, Phys. Rev. B **80**, 235205 (2009).

[20] W. M. Kim, I. H. Kim, J. H. Ko, B. Cheong, T. S. Lee, K. S. Lee, D. Kim, and T.-Y. Seong, J. Phys. D: Appl. Phys. **41**, 195409 (2008).

[21] J. Tang, L. Y. Deng, C. B. Tay, X. H. Zhang, J. W. Chai, H. Qin, H. W. Liu, T. Venkatesan, and S. J. Chua, J. Appl. Phys. **115**, 033111 (2014).

[22] G. Karczewski, T. Wojtowicz, Y.-J. Wang, X. Wu, and F. Peeters, Physica Stat. Sol. B **229**, 597 (2002).

[23] A. Tsukazaki, A. Ohtomo, M. Kawasaki, S. Akasaka, H. Yuji, K. Tamura, K. Nakahara, T. Tanabe, A. Kamisawa, T. Gokmen, et al., Phys. Rev. B **78**, 233308 (2008).

[24] W. Kohn, Physical Review **123**, 1242 (1961), ISSN 0031-899X.

[25] S. S. Krishtopenko, A. V. Ikonnikov, M. Orlita, Y. G. Sadofyev, M. Goiran, F. Teppe, W. Knap, and V. I. Gavrilenko, Journal of Applied Physics **117**, 112813 (2015), ISSN 0021-8979.

[26] Y. Zhang and S. Das Sarma, Phys. Rev. Lett. **95**, 256603 (2005).

[27] M. Padmanabhan, T. Gokmen, N. C. Bishop, and M. Shayegan, Phys. Rev. Lett. **101**, 026402 (2008).

[28] K. Han, N. Tang, J. D. Ye, J. X. Duan, Y. C. Liu, K. L. Teo, and B. Shen, Appl. Phys. Lett. **100**, 192105 (2012).

[29] K. Button, D. Cohn, M. von Ortenbert, B. Lax, E. Mollwo, and R. Helbig, Phys. Rev. Lett. **28**, 1637 (1972).

[30] J. Lloyd-Hughes, H. E. Beere, D. A. Ritchie, and M. B. Johnston, Phys. Rev. B **77**, 125322 (2008).

[31] J. Hodby, G. Russell, F. Peeters, J. Devreese, and D. Larsen, Phys. Rev. Lett. **58**, 1471 (1987).

[32] S. Das Sarma, Phys. Rev. Lett. **52**, 859 (1984).

[33] F. Peeters and J. Devreese, Phys. Rev. B **34**, 7246 (1986).

[34] G. D. Mahan and J. J. Hopfield, Physical Review Letters **12**, 241 (1964).
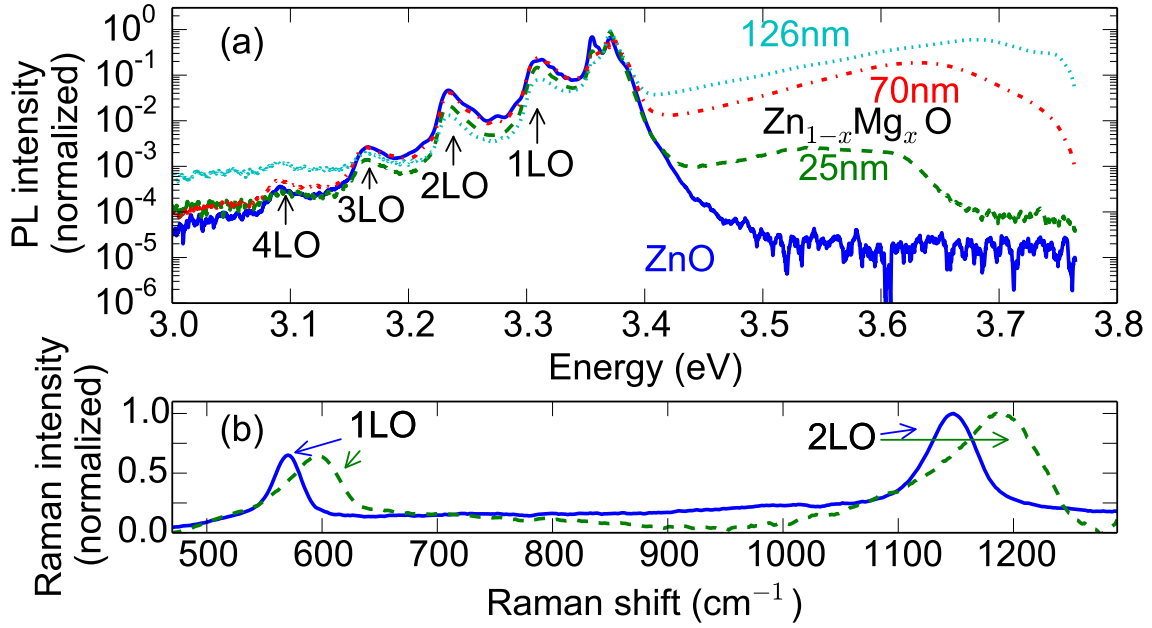
[35] S. Miyake, Phys. Rev. **170**, 726 (1968).

FIG. 1. (a) Photoluminescence (PL) spectra at $77\,\mathrm{K}$ under excitation at $325\,\mathrm{nm}$, normalized to the excitonic DX peak of ZnO (at $E_{\mathrm{DX}}=3.38\,\mathrm{eV}$). Raman emission peaks from harmonics of the LO phonons in ZnO are labelled nLO. The PL emission from the $\mathrm{Zn}_{1-x}\mathrm{Mg}_x\mathrm{O}$ layer is broad, and the energy gap increases with thickness owing to an increase in x. (b) Resonant Raman spectra around 1LO and 2LO show a blueshift in LO-phonon frequencies for the $25\,\mathrm{nm}$ film (dashed line) in comparison to the ZnO reference film (solid line).

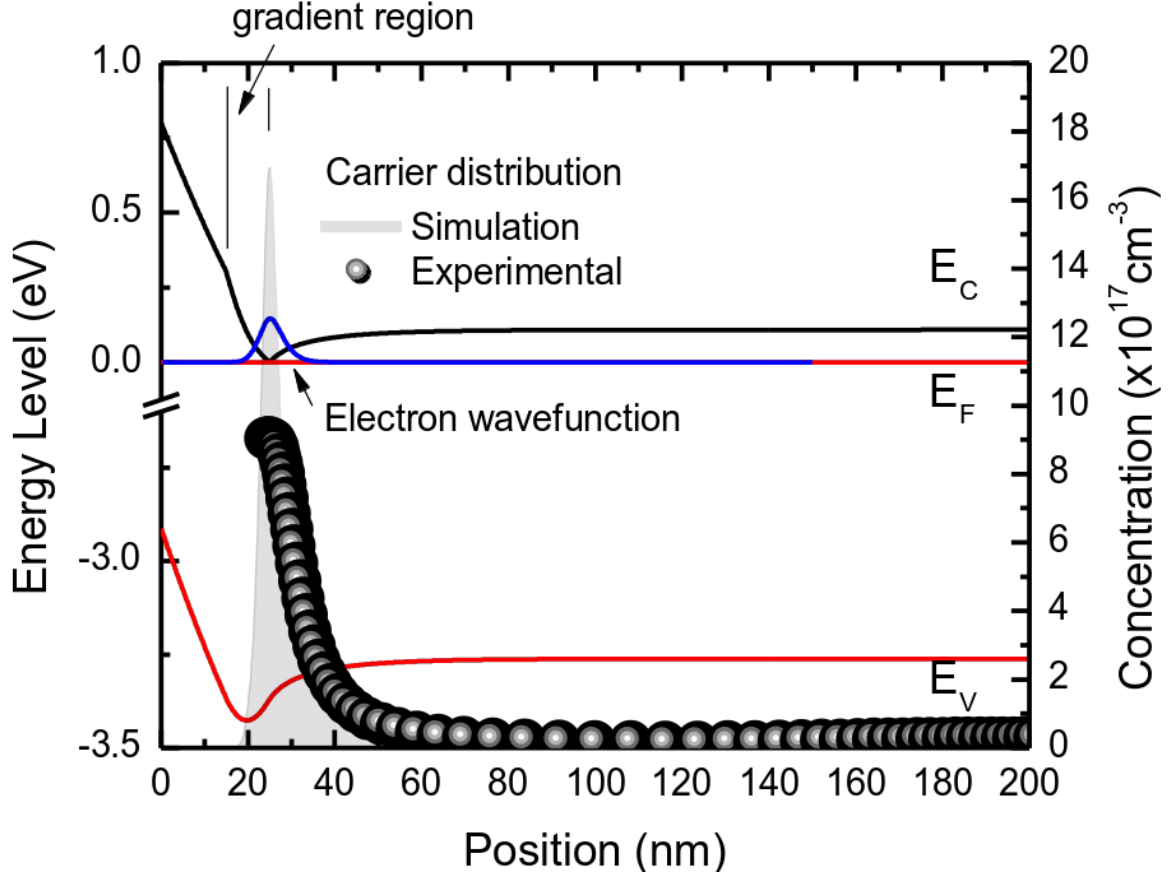[36]K. Nagasaka, Phys. Rev. B **15**, 2273 (1977).

FIG. 2. Self-consistent electronic bandstructure close to the interface of a $25\,\mathrm{nm}$ $\mathrm{Zn_{0.84}Mg_{0.16}O}$ layer grown on ZnO. The Mg content was assumed to grade linearly from $x = 0.16$ at $15\,\mathrm{nm}$ to $x = 0$ at $25\,\mathrm{nm}$. The calculated electron density is shown by the shaded area, while the points show experimental densities derived from the capacitance-voltage method.
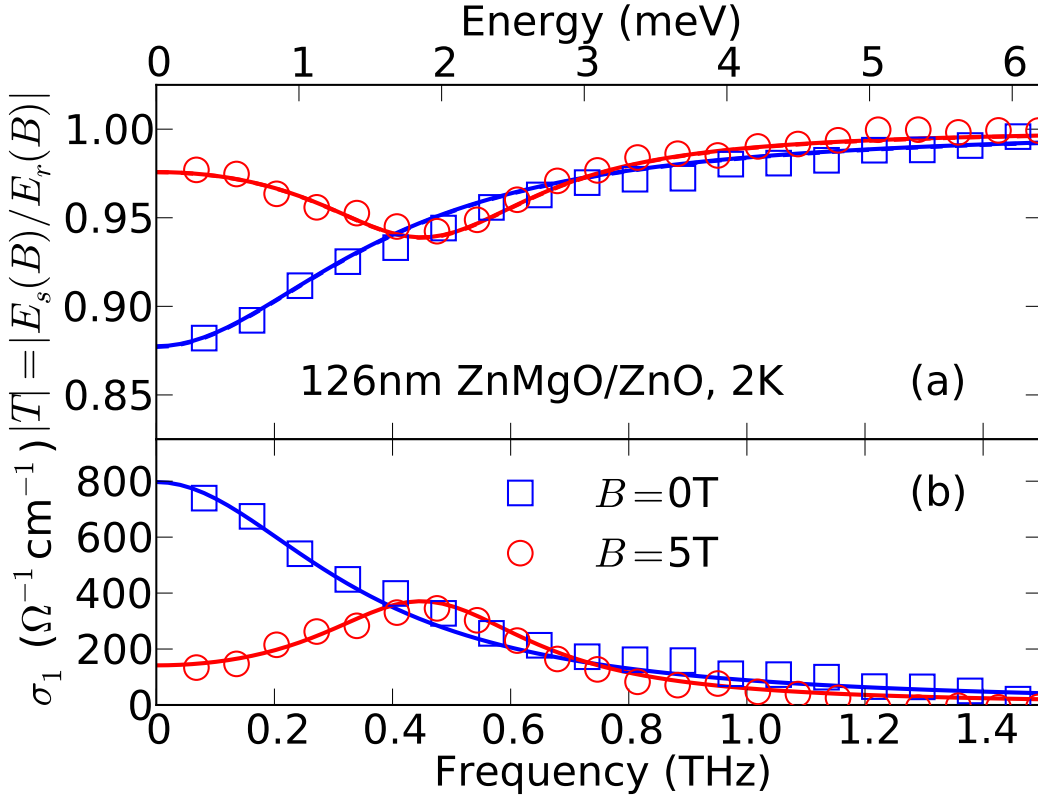
FIG. 3. (a) Amplitude transmission $|T|$ of a $126\,\mathrm{nm}$ $\mathrm{Zn}_{1-x}\mathrm{Mg}_x\mathrm{O}/\mathrm{ZnO}/\mathrm{sapphire}$ sample relative to $\mathrm{ZnO}/\mathrm{sapphire}$, at $2\,\mathrm{K}$ and magnetic fields $B = 0$ (squares) and $B = 5\,\mathrm{T}$ (circles). (b) Real part of the magnetoconductivity σ_1 calculated from the data in (a). Solid lines indicate fits with the Drude-Lorentz magnetoconductivity, yielding the polaron mass, density and scattering time.
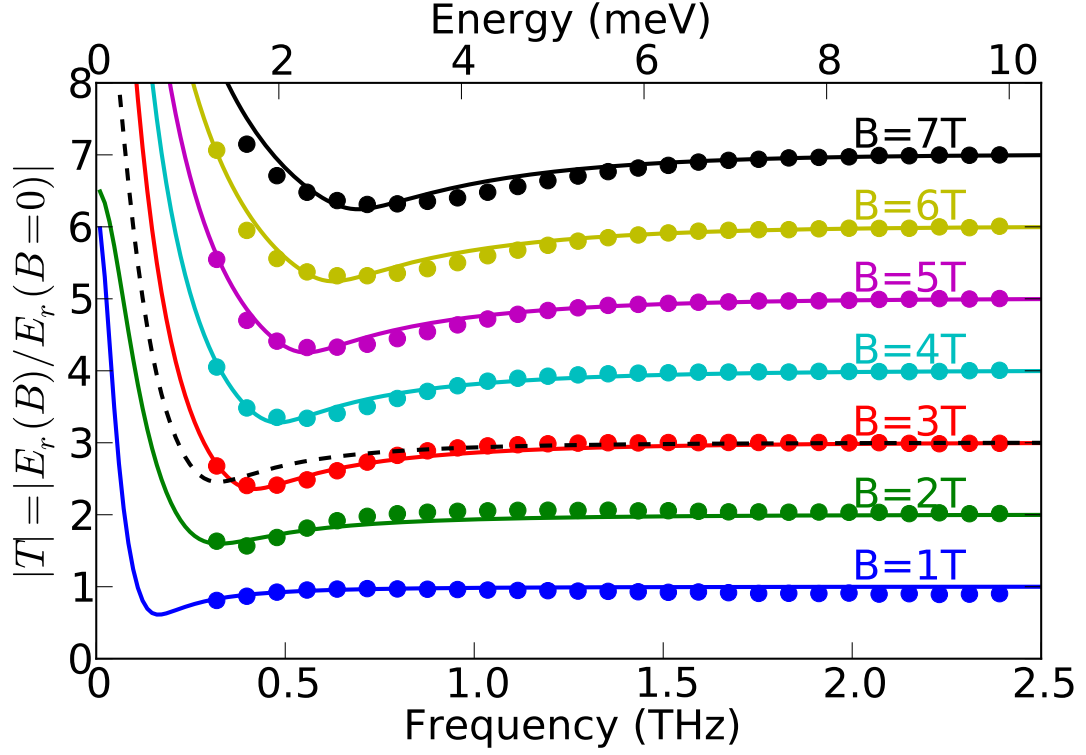
FIG. 4. Amplitude transmission of the ZnO/sapphire reference at magnetic fields B relative to that at $B = 0$. Experimental spectra (points) and fits using the transmission matrix method (solid lines, vertically offset by integers for clarity). The fits used a global N, and allowed m^* and τ to vary with B. The dashed line indicates the best fit at $B = 3\,\mathrm{T}$ with $m^* = 0.29\,m_e$, and varying N and τ.
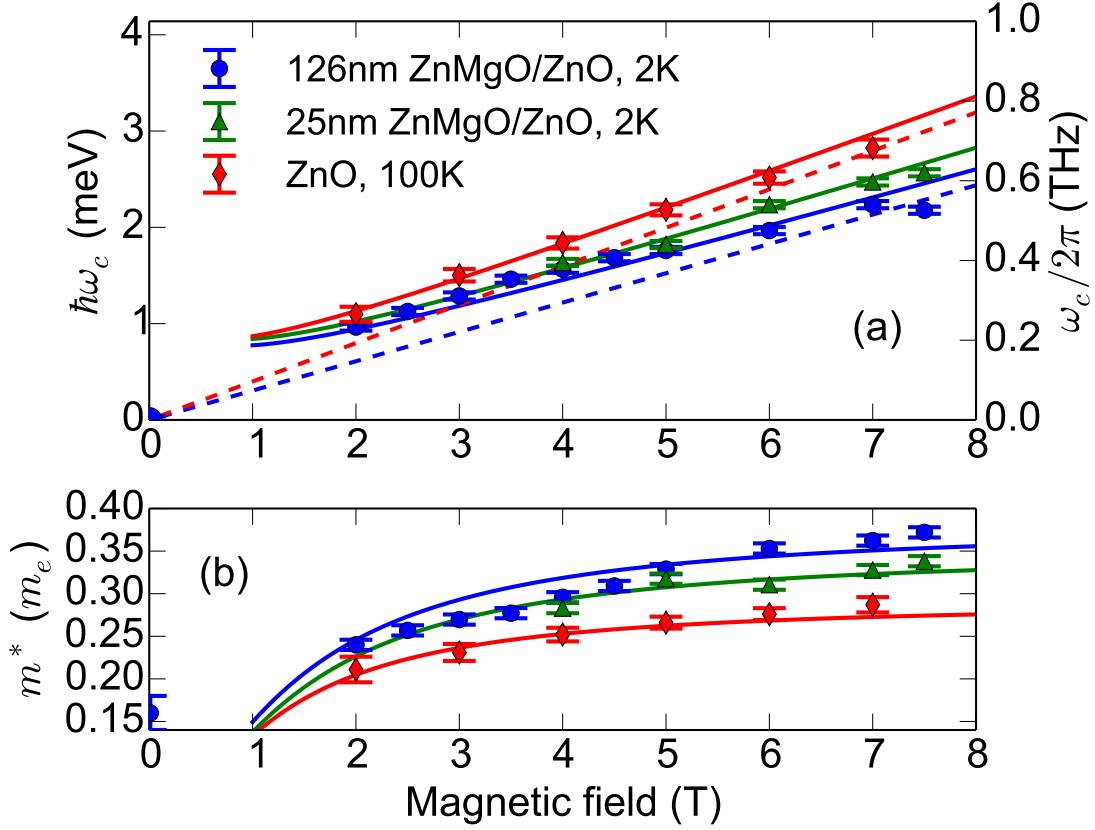
FIG. 5. (a) Cyclotron frequency $\omega_c(B)$ for interfacial polarons at $2\,\mathrm{K}$ in the $126\,\mathrm{nm}$ $\mathrm{Zn_{1-x}Mg_xO/ZnO}$ (circles) and $25\,\mathrm{nm}$ $\mathrm{Zn_{1-x}Mg_xO/ZnO}$ (triangles) samples, and for bulk-like polarons at $100\,\mathrm{K}$ (diamonds). Dashed lines show $\omega_c = eB/m^*$ with $m^* = 0.29\,m_e$ (red) or $m^* = 0.38\,m_e$ (blue). (b) Cyclotron masses vs B, as in (a). Calculated acoustic magnetopolaron dispersions are shown for the $126\,\mathrm{nm}$ $\mathrm{Zn_{1-x}Mg_xO/ZnO}$ (blue line), $25\,\mathrm{nm}$ $\mathrm{Zn_{1-x}Mg_xO/ZnO}$ (green line) and bulk-like ZnO (red line) samples. Error bars show the standard error in the fit parameter.